

**Failure analysis of
climate simulation
crashes**

D. D. Lucas et al.

Failure analysis of parameter-induced simulation crashes in climate models

D. D. Lucas¹, R. Klein^{1,2}, J. Tannahill¹, D. Ivanova¹, S. Brandon¹, D. Domyancic¹, and Y. Zhang¹

¹Lawrence Livermore National Laboratory, Livermore, CA, USA

²Department of Astronomy, University of California, Berkeley, CA 94720, USA

Received: 3 January 2013 – Accepted: 9 January 2013 – Published: 24 January 2013

Correspondence to: D. D. Lucas (ddlucas@alum.mit.edu)

Published by Copernicus Publications on behalf of the European Geosciences Union.

[Title Page](#)

[Abstract](#)

[Introduction](#)

[Conclusions](#)

[References](#)

[Tables](#)

[Figures](#)

[⏪](#)

[⏩](#)

[◀](#)

[▶](#)

[Back](#)

[Close](#)

[Full Screen / Esc](#)

[Printer-friendly Version](#)

[Interactive Discussion](#)



Abstract

5 Simulations using IPCC-class climate models are subject to fail or crash for a variety of reasons. Quantitative analysis of the failures can yield useful insights to better understand and improve the models. During the course of uncertainty quantification (UQ) ensemble simulations to assess the effects of ocean model parameter uncertainties on climate simulations, we experienced a series of simulation crashes within the Parallel Ocean Program (POP2) component of the Community Climate System Model (CCSM4). About 8.5% of our CCSM4 simulations failed for numerical reasons at combinations of POP2 parameter values. We apply support vector machine (SVM) classification from machine learning to quantify and predict the probability of failure as a function of the values of 18 POP2 parameters. A committee of SVM classifiers readily predicts model failures in an independent validation ensemble, as assessed by the area under the receiver operating characteristic (ROC) curve metric ($AUC > 0.96$). The causes of the simulation failures are determined through a global sensitivity analysis. Combinations of 8 parameters related to ocean mixing and viscosity from three different POP2 parameterizations are the major sources of the failures. This information can be used to improve POP2 and CCSM4 by incorporating correlations across the relevant parameters. Our method can also be used to quantify, predict, and understand simulation crashes in other complex geoscientific models.

20 1 Introduction

Modern global three-dimensional climate models are extraordinarily complex pieces of science (e.g. Randall et al., 2007; Gent et al., 2011; The HadGEM2 Development Team, 2011) and software engineering (Easterbrook et al., 2011; Rugaber et al., 2011; Easterbrook, 2010). They contain over a million lines of code (Easterbrook and Johns, 2009; Easterbrook, 2012) and use hundreds to thousands of files, functions, and sub-routines to solve equations of state and conservation laws for the flows of matter,

GMDD

6, 585–623, 2013

Failure analysis of climate simulation crashes

D. D. Lucas et al.

Title Page

Abstract

Introduction

Conclusions

References

Tables

Figures

⏪

⏩

◀

▶

Back

Close

Full Screen / Esc

Printer-friendly Version

Interactive Discussion



energy, and momentum within and between the atmosphere, oceans, land, and other reservoirs of the Earth system (Washington and Parkinson, 2005). They also use numerous algorithms of biological, chemical, geologic, and anthropogenic processes to simulate the cycles of carbon, nitrogen, sulfur, aerosols, ozone, greenhouse gases, and other climate-relevant quantities of interest. To compound this complexity, these algorithms operate across many orders of magnitude in space and time, and contain constituents that exist in gas, liquid, solid and mixed phases.

Given this enormous range of scientific complexity, climate models are vulnerable to many types of software design and implementation issues. Climate models are developed in a manner analogous to large open source and agile software projects (Easterbrook and Johns, 2009). Based on current best understanding, small groups of scientists create, test, and refine modules for select climate processes or sub-systems (e.g. atmospheric convection or aerosol microphysics). Their software changes are committed upstream to the climate model codebase, and the cycle is repeated until the model simulations reproduce desired features (i.e. model validation). Varying amounts of software testing are conducted throughout the cycle, but formal code verification practices (e.g. see D'Silva et al., 2008) are only recently starting to be considered for climate model development (Clune and Rood, 2011; Farrell et al., 2011). Nonetheless, the concentration on sound science, as opposed to software correctness, has led to climate models that contain fewer software defects than other comparably-sized projects (Pipitone and Easterbrook, 2012).

Software issues aside, many potential problems still arise with scientific representations in complex models. As code verification can be used to find software bugs, emerging tools being developed in the field of uncertainty quantification (UQ) (see National Research Council Report, 2012) can help pinpoint scientific discrepancies in simulation models, the knowledge of which can be used to guide and improve model development. Primary UQ targets for climate models are schemes containing parameters with adjustable values. These schemes represent processes that are not fully understood or cannot be directly simulated at the model resolutions of interest (e.g.

Failure analysis of climate simulation crashes

D. D. Lucas et al.

Title Page

Abstract

Introduction

Conclusions

References

Tables

Figures



Back

Close

Full Screen / Esc

Printer-friendly Version

Interactive Discussion



Stensrud, 2009). Parameterizations like this are often developed in isolation, so they can respond in unexpected ways when inserted in nonlinear climate models and coupled to other parameterizations. Small perturbations to the values of the adjustable parameters can amplify and lead to large changes in simulation outputs. In some cases, the simulations may fail altogether.

We report here on a series of simulation crashes encountered while running perturbed parameter UQ ensembles of the Community Climate System Model Version 4 (CCSM4) (Gent et al., 2011; CCSM4, 2012). Treating the problem as a black box in which we know only the values of the input parameters and a binary outcome flag indicating whether the simulations ultimately failed or completed, information that does not require detailed scientific knowledge, we present a method that successfully predicts crashes in independent simulations and pinpoints the model parameters causing the failures. We expect that our failure analysis method may be beneficial to understanding and improving other complex, geoscientific models.

2 Overview of climate simulations

Different sets of perturbed parameter UQ ensembles were executed as part of a broad effort to quantify and constrain uncertainties in the atmospheric, sea ice, and ocean model components of CCSM4 (Gent et al., 2011). The failures reported here occurred during simulations that perturbed parameter values in the Parallel Ocean Program (POP2), the ocean component of CCSM4. For these experiments, POP2 was coupled with the sea ice model, while data-based components were used for the land and atmosphere. The simulations were integrated for 10 yr, and the system was forced with climatological air-sea flux data using normal year forcing from Large and Yeager (2009). Further details about POP2 and the UQ ensembles are given below.

Failure analysis of climate simulation crashes

D. D. Lucas et al.

Title Page

Abstract

Introduction

Conclusions

References

Tables

Figures



Back

Close

Full Screen / Esc

Printer-friendly Version

Interactive Discussion



2.1 Ocean model and parameters

POP2 is a state of the art depth-level ocean model of the general ocean circulation that solves the 3-D primitive equations of rotational fluid dynamics and thermodynamics with standard approximations of Boussinesq and hydrostatics. It is developed and maintained at Los Alamos National Laboratory (Smith et al., 2010) and is the ocean component of CCSM4 developed at National Center for Atmospheric Research (Gent et al., 2011; Danabasoglu et al., 2012). The current simulations use the displaced-pole coordinate grid with the pole centered over Greenland and have a nominal horizontal resolution of 1°. Vertically it resolves 60 depth levels with resolution varying from 10 m in the upper ocean (surface to 200 m) to 250 m in the deeper ocean. Refer to Smith et al. (2010) and Danabasoglu et al. (2012) for more information.

The ocean model parameters perturbed in this study were selected by POP2 model developers. They are used in six different sub-grid scale parameterizations to simulate the effects of horizontal and vertical turbulent mixing in the oceans. The parameters and their uncertainty ranges are summarized in Table 1. Parameters 1–6 are used to capture horizontal mixing of momentum with spatially anisotropic viscosity (Large et al., 2001; Smith and McWilliams, 2003). Parameters 7–9 are used for horizontal mixing of tracers via isopycnal eddy-induced transport (Gent and McWilliams, 1990). Parameters 10–12 are used in recently developed schemes to simulate sub-mesoscale and mixed-layer eddies (Fox-Kemper et al., 2008) and abyssal tidal mixing (Jayne, 2009). Parameters 13–18 are used for vertical convection and vertical mixing with the K-Profile Parameterization (KPP) scheme (Large et al., 1994).

2.2 UQ ensembles

Table 2 summarizes the UQ ensemble simulations. Three separate studies were conducted, each consisting of 180 simulations. Out of 540 total simulations, there were 46 failures, with the failures occurring at various times during the integration period. Each of the three studies sampled the values of the 18 POP2 parameters simultaneously

GMDD

6, 585–623, 2013

Failure analysis of climate simulation crashes

D. D. Lucas et al.

Title Page

Abstract

Introduction

Conclusions

References

Tables

Figures



Back

Close

Full Screen / Esc

Printer-friendly Version

Interactive Discussion



using a space-filling Latin hypercube design (Helton and Davis, 2003). Parameter values were normalized to [0, 1] using the ranges (low and high values) and scales (linear and logarithm) noted in Table 1 and sampled as standard uniform probability distribution functions. The sample point coverage is illustrated in Figs. 1 and 2 for four parameters in one and two dimensions.

Ensembles were generated using the Lawrence Livermore National Laboratory UQ Pipeline (Walter, 2010; Tannahill et al., 2011), which is a Python-based scientific workflow system for running and analyzing concurrent UQ simulations on high performance computers. Using a simple, non-intrusive interface to simulation models, it provides strategies for sampling high dimensional uncertainty spaces, analyzing ensemble output, constructing surrogate approximation models (e.g. Forrester et al., 2008), incorporating observational data, performing statistical inferences, and estimating parameter values and probability distributions using maximum likelihood and Bayesian methods. Of the many capabilities provided by the UQ Pipeline, the failure analysis presented here uses the simulation parameter values and a method for calculating parameter sensitivities.

3 Descriptive failure analysis

Figures 1 and 2 show simulation successes and failures for the three Latin hypercube studies (540 runs) as a function of the values of 4 of the 18 parameters sampled in POP2. Similar figures were generated for the other parameters, but are not displayed to keep the discussion brief and because the failures are highly sensitive to changes in these parameters (see Sect. 5). It is not possible to directly visualize the dependencies in high dimensions, so the figures show the outcomes projected in one and two parameter dimensions (Figs. 1 and 2, respectively).

From the figures it is clear that the failures are generally concentrated around high values of parameters `vconst_corr` and `vconst_2`, and at low values of `backgrnd_vdc1`. A weaker dependence of the failures on high values of

Failure analysis of climate simulation crashes

D. D. Lucas et al.

Title Page

Abstract

Introduction

Conclusions

References

Tables

Figures



Back

Close

Full Screen / Esc

Printer-friendly Version

Interactive Discussion



`convect_corr` is also apparent. The analysis presented in following sections does not require a detailed understanding of the physical reasons that connect parameter values to simulation failures, though we briefly summarize the connections to help with the interpretation.

The parameters `vconst_corr` and `vconst_2` are part of the anisotropic horizontal viscosity parameterization applied to the momentum equations in POP2 (Smith et al., 2010). Their values are subject to 3 main constraints, considering the physical processes and limitations to maintain numerical stability; their lower bounds are constrained by the grid Reynolds number representing the ratio between advection and diffusion, the Munk boundary layer constraint is needed to represent western boundary currents (Jochum et al., 2008), and their upper bounds are limited by a linear diffusion stability requirement specified by a viscous Courant–Friedrichs–Lewy (CFL) condition, which depends on the integration time step (one hour in this study) and grid resolution (Griffies, 2004; Large et al., 2001). High values of these parameters may trigger the limit set by the CFL condition and is the likely reason for the model failures seen in the experiments. The `bckgrnd_vdc1` parameter is used to set the background diffusivity for diapycnal mixing from internal waves in the KPP vertical mixing parameterization (Large et al., 1994). Reducing the values of `bckgrnd_vdc1` and other `bckgrnd` parameters increase the numerical noise in the solution and consequently cause numerical instability. Similarly, increasing the value of `convect_corr`, which increases diffusivity and viscosity in the implicit KPP vertical mixing scheme, leads to instabilities in the vertical density profile. For detailed descriptions of all the POP2 parameters used in the current study please refer to Smith and McWilliams (2003), Large et al. (2001), and Danabasoglu et al. (2012).

In spite of the obvious relationships between the parameter values and simulation outcomes, other features present in the figures suggest that the ability to determine the causes of the failures is potentially complicated. Figure 2, for instance, indicates that there are strong correlations between failed simulations and pairs of parameter values. As one example, failures occur at the combination of high values of `vconst_corr` and

Failure analysis of climate simulation crashes

D. D. Lucas et al.

Title Page

Abstract

Introduction

Conclusions

References

Tables

Figures



Back

Close

Full Screen / Esc

Printer-friendly Version

Interactive Discussion



low values of `backgrnd_vdc1`. These two parameters reside in different modules in POP2 (`hmix_aniso`, and `vmix_kpp`, respectively), which makes it difficult for POP2 model developers and users to discover and attribute simulation failures to correlations in these parameters.

5 A more important complication arises from the overlap of simulation successes and failures in the low dimensional projections shown in the figures. Some simulations appear to fail in the same general vicinity of parameter space where other simulations succeed, and vice versa. To illustrate, the upper right portion of the scatterplot between `vconst_corr` and `vconst_2` in Fig. 2 contains a high density of failures and
10 successes. Another notable example is the isolated failure event shown in the lower left hand corner of the same scatterplot.

These overlaps can lead to serious misclassification errors in statistical models used to predict failures as a function of parameter values. Two types of misclassification errors can occur. Simulations that are predicted to fail, but actually succeed are false positives or type I errors; those that are predicted to succeed, but actually fail are false negatives or type II errors (see Sect. 4 for further details). Imbalanced data, in which the population of one class greatly outnumbers the populations of other classes, are associated with class overlap (Prati et al., 2004), and the POP2 outcomes are highly imbalanced (i.e. 46 failures out of 540 simulations). Another related explanation
20 is that higher parameter dimensions, and possibly a non-linear decision boundary, are required to effectively separate the outcomes.

Statistical approaches more powerful than the descriptive relationships illustrated in Figs. 1 and 2 are therefore needed to attack our problem. As described in the remaining sections, we turn to algorithms and diagnostics developed in the fields of pattern
25 recognition, machine learning, and signal detection. These methods provide us with the ability to predict simulation failures in advance of running the model and a tool to quantify the causes of the failures. This latter capability can be used to improve POP2 by making it more robust to parameter changes.

GMDD

6, 585–623, 2013

Failure analysis of climate simulation crashes

D. D. Lucas et al.

Title Page

Abstract

Introduction

Conclusions

References

Tables

Figures



Back

Close

Full Screen / Esc

Printer-friendly Version

Interactive Discussion



4 Probabilistic failure classification

For a given set of model input parameters, a POP2 simulation will either succeed or fail. We denote these outcomes by a two-class categorical variable in which failures belong to class C_f and successes belong to class C_s . The present discussion considers only a single failure class, but we recognize that simulations can fail for a variety of reasons (e.g. lack of iterative convergence, numerical instabilities, etc). Without difficulty, the two-class methodology described below can be extended to handle multiple modes of failure.

Our goal for probabilistic failure classification is to determine the probability that a POP2 simulation will fail for a vector of model input parameters $\mathbf{x} = (x_1, x_2, \dots, x_{18})$. We denote this using the conditional probability $\mathcal{P}(C_f|\mathbf{x})$. Using Bayes' rule, the posterior conditional probability can be written

$$\mathcal{P}(C_f|\mathbf{x}) = \frac{\mathcal{P}(\mathbf{x}|C_f)\mathcal{P}(C_f)}{\mathcal{P}(\mathbf{x}|C_f)\mathcal{P}(C_f) + \mathcal{P}(\mathbf{x}|C_s)\mathcal{P}(C_s)}, \quad (1)$$

where $\mathcal{P}(\mathbf{x}|C_j)$ and $\mathcal{P}(C_j)$ correspond to class-conditional densities and class priors, respectively. By introducing a variable λ representing the natural logarithm of the likelihood-odds ratio,

$$\lambda = \ln \left[\frac{\mathcal{P}(\mathbf{x}|C_f)}{\mathcal{P}(\mathbf{x}|C_s)} \frac{\mathcal{P}(C_f)}{\mathcal{P}(C_s)} \right], \quad (2)$$

Eq. (1) can be rewritten as the “S-shaped” logistic sigmoid function

$$\mathcal{P}(C_f|\mathbf{x}) = \frac{1}{1 + \exp(-\lambda)}. \quad (3)$$

The λ term is a function of \mathbf{x} and takes values in $(-\infty, \infty)$. As illustrated in Fig. 3, the sigmoid function is bounded between 0 and 1, inclusive. This formalism provides a mechanism to transform an input vector of model parameter values to a probability that the corresponding simulation will fail or succeed.

Failure analysis of climate simulation crashes

D. D. Lucas et al.

Title Page

Abstract

Introduction

Conclusions

References

Tables

Figures

⏪

⏩

◀

▶

Back

Close

Full Screen / Esc

Printer-friendly Version

Interactive Discussion



4.1 SVM classification

Support vector machine (SVM) classification (Vapnik, 1995; Cortes and Vapnik, 1995; Burges, 1998) from the fields of pattern recognition and supervised machine learning (Bishop, 2007; Kotsiantis, 2007) is used to assign a simulation to class C_f or C_s for input vector \mathbf{x} . Briefly, the SVM method is based on maximizing the distance between hyperplanes that separate the classes (i.e. the margin), while allowing for misclassifications from overlapping data points during training (i.e. a soft margin). For non-linearly separable classes, the hyperplanes are determined by transforming the input space to a higher-dimensional feature space using kernel functions. The purpose of the transformation is to make it easier to separate the classes, as illustrated conceptually in Fig. 4. The support vectors are the training points that lie on the hyperplanes of the optimized margin. New input vectors \mathbf{x} are assigned to a class using the sign of the predictive decision function

$$f(\mathbf{x}) = \sum_{i=1}^{N_s} y_i \alpha_i K(\mathbf{x}_i, \mathbf{x}) + b, \quad (4)$$

where $f(\mathbf{x}) > 0$ and $f(\mathbf{x}) < 0$ are assigned to classes C_f and C_s , respectively. The sum in Eq. (4) is over the N_s support vectors from the training set, $y_i \in \{-1, 1\}$ is a binary outcome indicator variable, $K(\mathbf{x}_i, \mathbf{x})$ is the kernel function, and b and α_i are, respectively, bias and Lagrange multiplier terms determined through constrained optimization of the margin. Refer to Burges (1998), Bishop (2007), or Chang and Lin (2011) for further details.

The decision function in Eq. (4) assigns inputs to a class, but does not provide a probability of class membership. An extension to the standard SVM approach was therefore developed (Platt, 1999) that derives class probabilities by fitting λ in Eq. (2) to a two parameter function using the training data and cross validation. A variation of this procedure is implemented in the LIBSVM package (Chang and Lin, 2011), which we use to calculate posterior failure probabilities, $\mathcal{P}(C_f|\mathbf{x})$. From this

GMDD

6, 585–623, 2013

Failure analysis of climate simulation crashes

D. D. Lucas et al.

Title Page

Abstract

Introduction

Conclusions

References

Tables

Figures



Back

Close

Full Screen / Esc

Printer-friendly Version

Interactive Discussion



package, we use the C -support version of SVM classification with Gaussian kernels, $K(\mathbf{x}_j, \mathbf{x}) = \exp(-\gamma \|\mathbf{x}_j - \mathbf{x}\|^2)$. The values of the two SVM training parameters, the kernel width ($\gamma = 0.1$) and the misclassification penalty ($C = 3$), were determined through grid search, bootstrapping, and optimization of classification performance metrics (see below).

The training set is comprised of 360 simulations from Latin hypercube studies 1 and 2 in Table 2. The remaining 180 simulations from Latin hypercube study 3 are used for testing and independent validation (see Sect. 4.3). There are 32 simulation failures and 328 successes in the training set. Given the relatively small ratio of the number of failure events to the number of classifier inputs, we utilize bootstrapping aggregation (i.e. “bagging”) (Breiman, 1996) to help improve the classification performance and to quantify the variability of the predicted class posterior probabilities. The bootstrapping is applied by resampling with replacement the training data $N_b = 100$ times. Each time, we draw a random selection of 80% of the training data to construct an individual classifier and use the remaining 20% for testing that classifier. The same SVM training parameters (γ and C) are used for all classifiers. Failure predictions are then based on a committee of classifiers

$$\mu_c = \frac{1}{N_b} \sum_{i=1}^{N_b} \mathcal{P}_i(C_i|\mathbf{x}) \quad (5)$$

and

$$\sigma_c^2 = \frac{1}{N_b} \sum_{i=1}^{N_b} [\mathcal{P}_i(C_i|\mathbf{x}) - \mu_c]^2, \quad (6)$$

where μ_c and σ_c are the mean and standard deviation of the committee.

Failure analysis of climate simulation crashes

D. D. Lucas et al.

Title Page

Abstract

Introduction

Conclusions

References

Tables

Figures



Back

Close

Full Screen / Esc

Printer-friendly Version

Interactive Discussion



4.2 Classification performance

Using a format known as the “confusion matrix” in machine learning, Fig. 5 summarizes the four possible outcomes for the two-class simulation failure problem. Classifiers that correctly predict actual failures and successes are labeled true positives (TP) and true negatives (TN), respectively; those that incorrectly predict actual failures and successes are denoted false negatives (FN) and false positives (FP), respectively. Of the numerous ways to combine these outcomes to assess classifier performance, we focus on the true positive rate (TPR) and false positive rate (FPR), which are given by the expressions

$$\text{TPR} = \frac{\text{TP}}{\text{TP} + \text{FN}}, \quad (7)$$

and

$$\text{FPR} = \frac{\text{FP}}{\text{FP} + \text{TN}}. \quad (8)$$

Perfect classifiers have TPR and FPR values of 1 and 0, respectively. As noted previously, we use a classifier committee that calculates an ensemble of probabilities of class membership. The assignment to a particular class and resulting TPR and FPR values therefore depends upon a specified decision variable and threshold value. If decisions are made using the committee average with a threshold of 0.5, for example, then μ_c values above and below this value will be assigned to classes C_f and C_s , respectively.

The quantities in Eqs. (7) and (8) are combined into a convenient diagram used in signal detection and decision analysis known as a receiver operating characteristic (ROC) curve (Swets, 1988; Fawcett, 2006). ROC curves plot the FPR (horizontal axis) versus TPR (vertical axis) of a decision variable as the threshold is varied from $+\infty$ to $-\infty$. A perfect classifier is represented in ROC space by the vertical line connecting points (0, 0) and (0, 1), followed by the horizontal line connecting points (0, 1) and (1, 1).

Failure analysis of climate simulation crashes

D. D. Lucas et al.

Title Page

Abstract

Introduction

Conclusions

References

Tables

Figures

◀

▶

◀

▶

Back

Close

Full Screen / Esc

Printer-friendly Version

Interactive Discussion



A classifier that makes random assignments, on the other hand, is represented by the diagonal line connecting points (0, 0) and (1, 1). The predictive capability of a classification system can therefore be assessed by a single number, the area under the ROC curve (AUC) (e.g. Marzban, 2004). As a rough rule of thumb, a classifier with an AUC score of about 0.8 or higher is useful for discrimination.

Figure 6 shows the ROC curve for the collection of test sets aggregated from the bootstrapping procedure using the failure probabilities of the individual classifiers as the decision variable. The aggregated test set has 7200 data instances (0.2 test fraction \times 360 POP2 simulations \times 100 bootstrapped resampling size). The SVM fitting parameters (γ and C) were selected during the training phase to maximize the AUC score shown in the figure. The resulting AUC of 0.93 suggests that the classifiers should have excellent predictive capability, which we confirm through independent validation.

4.3 Independent validation

To demonstrate the ability to predict simulation failures, we conducted an independent validation study using 180 additional POP2 Latin hypercube simulations that were not used to train the classifiers (study 3 in Table 2). Before running the simulations, the mean and standard deviation of failure probabilities were calculated from the committee for each run using Eqs. (5) and (6). Runs were assigned to C_f using decision criteria denoted by

$$D \equiv \text{variable} \geq \text{threshold}. \quad (9)$$

Two initial criteria were selected using the same threshold, but different decision variables. The first criterion used the committee average

$$D_{\text{avg}} \equiv \mu_c \geq 0.5, \quad (10)$$

while the second used the sum of the committee average and standard deviation

$$D_{\text{sum}} \equiv \mu_c + \sigma_c \geq 0.5. \quad (11)$$

The second criterion was chosen to account for variability across committee members by categorizing some simulations as C_f even though they had a committee mean below 0.5. After all of the simulations completed, a third criterion based on the signal-to-noise ratio from the committee, D_{snr} , was also considered and analyzed (see below).

The resulting predictions and actual outcomes are summarized in Table 3 and displayed in Figs. 7 and 8. As noted in Table 2, there were 14 actual simulation failures and 166 successes in the study. The classifier committee performed exceedingly well using the two initial criteria, D_{avg} and D_{sum} . Referring to the confusion matrix in Fig. 7, both made 174 correct predictions (TP + TN, 96.7% accuracy) and only 6 incorrect predictions (FP + FN). The incorrect predictions, however, are distributed differently for the two criteria. D_{avg} had more FNs than FPs, while D_{sum} had an equal number of each. Because of this difference, D_{avg} and D_{sum} operate at different points in ROC space. D_{avg} has ROC coordinates of (1/166, 9/14), while D_{sum} operates at (3/166, 11/14). Based on their Euclidean distance from a perfect classifier, which is given by $\left[\text{FPR}^2 + (\text{TPR} - 1)^2 \right]^{1/2}$, we conclude that D_{sum} (distance = 0.215) performs better than D_{avg} (distance = 0.357).

To ascertain the cause of the performance difference between D_{sum} and D_{avg} , the top and middle panels of Fig. 8 display the μ_c and $\mu_c + \sigma_c$ decision variables for the runs in the independent validation set. The decision criteria are represented by the horizontal lines in the panels. Runs that are on or above the lines were predicted to fail, while those that actually failed are displayed in red (and those that succeeded in blue). The figure indicates, for example, that runs 17 and 120 failed, but were misclassified by D_{avg} because their μ_c values were slightly below 0.5. By comparison D_{sum} assigned these runs to the correct class, but also misdiagnosed runs 2 and 95. A visual inspection of the figure shows that, except for the relative position of the threshold, the distribution of points in μ_c and $\mu_c + \sigma_c$ look very similar. We therefore attribute the performance difference to the threshold value. If D_{avg} had used a threshold value of about 0.4 instead

Failure analysis of climate simulation crashes

D. D. Lucas et al.

Title Page

Abstract

Introduction

Conclusions

References

Tables

Figures

◀

▶

◀

▶

Back

Close

Full Screen / Esc

Printer-friendly Version

Interactive Discussion



these cases, the ROC curve for μ_c/σ_c is noticeably better and has an AUC of 0.966. This occurs because μ_c/σ_c is more effective at separating the classes, which enables it to identify more TPs as the threshold is lowered. Overall, however, all three decision variables perform exceedingly well at classifying new simulation failures. Using these ROC curves, we can choose decision criteria for making new predictions that consider the tradeoffs between TPs and FPs. Slightly lowering the threshold in D_{snr} , for example, will increase the TPR and move it to a point that lies closer to a perfect classifier in ROC space, but this occurs at the expense of also increasing the FPR.

5 Sensitivity analysis of simulation failures

Following on the demonstrated success of the independent validation study, we use the classifier committee to identify, quantify, and rank the importance of the model parameters responsible for the simulation failures. This information can be used to make the model more robust to parameter perturbations by improving the modules associated with the most sensitive parameters. For this analysis, we draw 10^4 Latin hypercube samples from uniform distributions representing the 18 POP2 parameters, calculate the average failure probability from a committee of classifiers (μ_c) at each of the sample points, and then perform a global sensitivity analysis (Saltelli et al., 2000; Helton et al., 2006) on the parameter-induced variance of $\log \mu_c$. All of the available simulation data are used to compute the parameter sensitivities by re-training a new committee of 100 SVM classifiers with the full set of 540 simulations from studies 1–3 in Table 1. The training follows the procedure previously described in Sect. 4.1 (i.e. bootstrap aggregation using 80% of the data for training and 20% for testing individual classifiers). Also note that the sensitivity analysis is illustrated below using μ_c as the committee response, but the same general results are obtained using the signal-to-noise ratio (μ_c/σ_c).

Parameter sensitivities are measured and ranked using Sobol indices (Sobol, 2001; Saltelli et al., 2000), which decompose the variance of $\log \mu_c$ into contributions from

GMDD

6, 585–623, 2013

Failure analysis of climate simulation crashes

D. D. Lucas et al.

[Title Page](#)

[Abstract](#)

[Introduction](#)

[Conclusions](#)

[References](#)

[Tables](#)

[Figures](#)



[Back](#)

[Close](#)

[Full Screen / Esc](#)

[Printer-friendly Version](#)

[Interactive Discussion](#)



individual parameters and various higher-order combinations of parameters. Polynomial chaos expansions (Wiener, 1938) provide a convenient format for the sensitivity analysis because the squares of the expansion coefficients are directly proportional to Sobol indices (Sudret, 2008; Lucas and Prinn, 2005; Tatang et al., 1997). The distribution of $\log \mu_c$ is fit to $N_p = 18$ parameters using a second-order polynomial chaos expansion expressed as

$$\log \mu_c = a_0 + \sum_{i=1}^{N_p} [b_i P_1(\xi_i) + c_i P_2(\xi_i)] + \sum_{i=1}^{N_p-1} \sum_{j=i+1}^{N_p} d_{ij} P_1(\xi_i) P_1(\xi_j), \quad (13)$$

where ξ_i is the random variable representation of parameter i , $P_n(\xi_i)$ is an n th order orthogonal polynomial in ξ_i , and the a_0 , b_i , c_i and d_{ij} are expansion coefficients to be determined. For the case where the ξ_i are standard uniform random variables, the $P_n(\xi_i)$ are the shifted Legendre polynomials (see Xiu and Karnidakis, 2002) with the following orthogonality property

$$\int_0^1 P_m(\xi_i) P_n(\xi_i) d\xi_i = \frac{1}{2n+1} \delta_{mn}, \quad (14)$$

where δ_{mn} is the Kronecker delta function. The first and second order shifted Legendre polynomials are given by

$$P_1(\xi_i) = 2\xi_i - 1 \quad (15)$$

and

$$P_2(\xi_i) = 6\xi_i^2 - 6\xi_i + 1. \quad (16)$$

The coefficients in Eq. (13) are determined through least squares, and higher-order terms are not considered because the second-order expansion fits the data very well

Failure analysis of climate simulation crashes

D. D. Lucas et al.

Title Page

Abstract

Introduction

Conclusions

References

Tables

Figures

◀

▶

◀

▶

Back

Close

Full Screen / Esc

Printer-friendly Version

Interactive Discussion



(adjusted $R^2 = 0.98$). The resulting fit is given in Table 4, which shows the leading terms of the expansion in two forms.

Analytical expressions for the moments of $\log \mu_c$ as a function of the POP2 parameters are derived by directly taking expectation values of Eq. (13). The average value and variance are

$$\text{avg}(\log \mu_c) = a_0, \quad (17)$$

and

$$\text{var}(\log \mu_c) = \underbrace{\sum_{i=1}^{N_p} \left(\frac{b_i^2}{3} + \frac{c_i^2}{5} \right)}_{\text{individual parameters}} + \underbrace{\sum_{i=1}^{N_p-1} \sum_{j=i+1}^{N_p} \frac{d_{ij}^2}{9}}_{\text{pairs of parameters}}. \quad (18)$$

The two groups of terms labeled on the right hand side of Eq. (18) signify variance contributions from individual parameters (linear and quadratic) and pairs of parameters. The fractional values of the squared polynomial chaos expansion coefficients in Eq. (18) follow from application of Eq. (14).

Given a parameter-based decomposition of the variance, we have developed a technique to visualize complex variance connections using network graphs with nodes and edges. The size of node i in the graph is proportional to the fractional contribution from parameter i ,

$$\text{node}_i \propto \frac{b_i^2/3 + c_i^2/5}{\text{var}(\log \mu_c)}, \quad (19)$$

while the thickness of edge $_{ij}$ connecting node i and node j is proportional to the fractional contribution from joint variations of parameters i and j ,

$$\text{edge}_{ij} \propto \frac{d_{ij}^2/9}{\text{var}(\log \mu_c)}. \quad (20)$$

Failure analysis of climate simulation crashes

D. D. Lucas et al.

Title Page

Abstract

Introduction

Conclusions

References

Tables

Figures



Back

Close

Full Screen / Esc

Printer-friendly Version

Interactive Discussion



Failure analysis of climate simulation crashes

D. D. Lucas et al.

[Title Page](#)

[Abstract](#)

[Introduction](#)

[Conclusions](#)

[References](#)

[Tables](#)

[Figures](#)



[Back](#)

[Close](#)

[Full Screen / Esc](#)

[Printer-friendly Version](#)

[Interactive Discussion](#)



The technique has been extended to include higher order effects (e.g. using edge $_{ijk}$ for 3rd-order terms), but this is not needed for the current application. Important parameters on the resulting network graph are represented by nodes that are large or make significant connections to other nodes.

Figure 10 displays the network graph for the variance decomposition of $\log \mu_c$. Based on node size and connectivity, the graph indicates that 8 out of the 18 parameters are the main drivers of the simulation failures (see parameters labeled in red in the graph). These 8 parameters account for about 95 % of the variance of $\log \mu_c$, as quantified using Eq. (18). Of these, `vconst_corr`, `vconst_2`, `convect_corr`, and `bckgrnd_vdc1` stand out distinctly as the top 4 parameters in the graph. Recall that the same 4 parameters are described in Sect. 3 and displayed in Figs. 1 and 2. The top 4 parameters have the largest overall and most heavily connected nodes in the graph, and they collectively account for about 88 % of the variance of $\log \mu_c$. The strong connections indicate that the probability of simulation failure depends on correlations between the top 4 parameters. The direction of the dependence is determined by inspecting the signs of the corresponding coefficients in the polynomial chaos expansion (i.e. for ξ_1 , ξ_2 , ξ_{13} , and ξ_{14}). Referring to Table 4, the failure probability increases for increasing values of `vconst_corr`, `vconst_2`, and `convect_corr`, and decreasing values of `bckgrnd_vdc1`, which is in accordance with the results in Figs. 1 and 2.

The variance decomposition therefore validates the descriptive relationships given in Sect. 3. However, it also extends the failure analysis in important ways. Equation (18) quantitatively ranks the effects of the parameters on the simulation failures, which provides a way to prioritize efforts to improve the model. This type of ranking cannot be easily obtained using just the scatterplots in Figs. 1 and 2. Moreover, the scatterplots show the correlations between the parameter values and simulation failures, but the one and two dimensional projections are not sufficient for separating the overlapping C_f and C_s classes. Figure 10, on the other hand, very clearly shows that four or more parameter dimensions are required to explain and separate the simulation failures from the successes.

6 Summary and conclusions

We experienced a series of code crashes while running Latin hypercube ensemble simulations that sampled the values of 18 ocean mixing and viscosity parameters in the POP2 component of CCSM4. The crashes occurred for numerical reasons at different combinations of parameter values, which we surmise is due to violations of numerical conditions defined in the model (e.g. CFL as described in Sect. 3). Assuming no special knowledge or physical insight about the specific nature of the crashes, we formulate the simulations as a binary problem (i.e. they fail or succeed) and use machine learning classification to quantify failure probabilities as a function of the 18 model parameters. A highly predictive classification system is trained from a dataset containing only 32 failure instances out of 360 simulations and validated using an independent set of 180 simulations. The resulting classification system has an area under the ROC curve exceeding 0.96 and achieves discrimination accuracies above 97 %. Global sensitivity analysis is then used to identify 8 model parameters from 4 different modules that drive high probabilities of failing, the results of which can be used to increase the robustness of CCSM4 to parameter perturbations and to characterize simulation failures in other complex scientific computer models.

Acknowledgements. Computing support for this work came from the Lawrence Livermore National Laboratory (LLNL) Institutional Computing Grand Challenge program. We thank G. Danabasoglu, M. Jochum, and R. Tokmakian for recommending the ocean model parameters and their uncertainty ranges. This work was performed under the auspices of the US Department of Energy by Lawrence Livermore National Laboratory under Contract DE-AC52-07NA27344, was funded by LLNL's Uncertainty Quantification Strategic Initiative Laboratory Directed Research and Development Project under tracking code 10-SI-013, and is released under UCRL number LLNL-JRNL-608873.

GMDD

6, 585–623, 2013

Failure analysis of climate simulation crashes

D. D. Lucas et al.

Title Page

Abstract

Introduction

Conclusions

References

Tables

Figures



Back

Close

Full Screen / Esc

Printer-friendly Version

Interactive Discussion



References

- Bishop, C. M.: Pattern Recognition and Machine Learning, Information Science and Statistics, 1st Edn., Springer, 2007. 594
- Breiman, L.: Bagging predictors, *Mach. Learn.*, 24, 123–140, 1996. 595
- 5 Burges, C. J. C.: A tutorial on support vector machines for pattern recognition, *Data Min. Knowl. Discov.*, 2, 121–167, 1998. 594
- CCSM4: The Community Climate System Model, Version 4, available at: <http://www.cesm.ucar.edu/models/ccsm4.0/> (last access: 22 January 2013), archived on 21 July 2010: <http://www.webcitation.org/5rOj1F8rL>, 2012. 588
- 10 Chang, C. C. and Lin, C. J.: LIBSVM: A library for support vector machines, *ACM Trans. Intell. Syst. Technol.*, 2, doi:10.1145/1961189.1961199, 2011. 594
- Clune, T. and Rood, R.: software testing and verification in climate model development, *IEEE Software*, 28, 49–55, 2011. 587
- Cortes, C. and Vapnik, V.: Support-vector networks, *Mach. Learn.*, 20, 273–297, 1995. 594
- 15 Danabasoglu, G., Bates, S., Briegleb, B., Jayne, S., Jochum, M., Large, W., Peacock, S., and Yeager, S.: The CCSM4 ocean component, *J. Clim.*, 25, 1361–1389, 2012. 589, 591
- D'Silva, V., Kroening, D., and Weissenbacher, G.: A survey of automated techniques for formal software verification, *IEEE T. Comput.-Aid. D.*, 27, 1165–1178, 2008. 587
- Easterbrook, S. M.: Climate change: a grand software challenge, in: *FoSER*, edited by: Roman, G.-C. and Sullivan, K. J., 99–104, ACM, 2010. 586
- 20 Easterbrook, S. M.: Do Over or Make Do? Climate Models as a Software Development Challenge, 2012 Fall Meeting Abstracts, IN14B-01, AGU, San Francisco, Calif., 3–7 December, 2012. 586
- Easterbrook, S. M. and Johns, T. C.: Engineering the software for understanding climate change, *Comput. Sci. Eng.*, 11, 65–74, 2009. 586, 587
- 25 Easterbrook, S. M., Edwards, P. N., Balaji, V., and Budich, R.: Guest editors' introduction: climate change – science and software, *IEEE Software*, 28, 32–35, 2011. 586
- Farrell, P. E., Piggott, M. D., Gorman, G. J., Ham, D. A., Wilson, C. R., and Bond, T. M.: Automated continuous verification for numerical simulation, *Geosci. Model Dev.*, 4, 435–449, doi:10.5194/gmd-4-435-2011, 2011. 587
- 30 Fawcett, T.: An introduction to ROC analysis, *Pattern Recogn. Lett.*, 27, 861–874, 2006. 596

Failure analysis of climate simulation crashes

D. D. Lucas et al.

Title Page

Abstract

Introduction

Conclusions

References

Tables

Figures



Back

Close

Full Screen / Esc

Printer-friendly Version

Interactive Discussion



Failure analysis of climate simulation crashes

D. D. Lucas et al.

[Title Page](#)

[Abstract](#)

[Introduction](#)

[Conclusions](#)

[References](#)

[Tables](#)

[Figures](#)

[⏪](#)

[⏩](#)

[◀](#)

[▶](#)

[Back](#)

[Close](#)

[Full Screen / Esc](#)

[Printer-friendly Version](#)

[Interactive Discussion](#)



- Forrester, A. I. J., Sobester, A., and Keane, A. J.: Engineering Design via Surrogate Modelling – A Practical Guide, Wiley, 2008. 590
- Fox-Kemper, B., Ferrari, R., and Hallberg, R.: Parameterization of mixed layer eddies. Part I: Theory and diagnosis, *J. Phys. Oceanogr.*, **38**, 1145–1165, 2008. 589
- 5 Gent, P. R. and McWilliams, J. C.: Isopycnal mixing in ocean circulation models, *J. Phys. Oceanogr.*, **20**, 150–155, 1990. 589
- Gent, P. R., Danabasoglu, G., Donner, L. J., Holland, M. M., Hunke, E. C., Jayne, S. R., Lawrence, D. M., Neale, R. B., Rasch, P. J., Vertenstein, M., Worley, P. H., Yang, Z.-L., and Zhang, M.: The Community Climate System Model Version 4, *J. Climate*, **24**, 4973–4991, 2011. 586, 588, 589
- 10 Griffies, S.: Fundamentals of Ocean Climate Models, Princeton University Press, 2004. 591
- Helton, J. C. and Davis, F. J.: Latin hypercube sampling and the propagation of uncertainty in analyses of complex systems, *Reliab. Eng. Syst. Safe.*, **81**, 23–69, 2003. 590
- Helton, J., Johnson, J., Sallaberry, C., and Storlie, C.: Survey of sampling-based methods for uncertainty and sensitivity analysis, *Reliab. Eng. Syst. Safe.*, **91**, 1175–1209, 2006. 600
- 15 Jayne, S. R.: The impact of abyssal mixing parameterizations in an ocean general circulation model, *J. Phys. Oceanogr.*, **39**, 1756–1775, 2009. 589
- Jochum, M., Danabasoglu, G., Holland, M., Kwon, Y.-O., and Large, W. G.: Ocean viscosity and climate, *J. Geophys. Res.*, **113**, C06017, doi:10.1029/2007JC004515, 2008. 591
- 20 Kotsiantis, S. B.: Supervised Machine Learning: a Review of Classification Techniques, in: Proceedings of the 2007 conference on Emerging Artificial Intelligence Applications in Computer Engineering: Real World AI Systems with Applications in eHealth, HCI, Information Retrieval and Pervasive Technologies, IOS Press, Amsterdam, The Netherlands, The Netherlands, 3–24, 2007. 594
- 25 Large, W. and Yeager, S.: The global climatology of an interannually varying air–sea flux data set, *Clim. Dynam.*, **33**, 341–364, 2009. 588
- Large, W. G., McWilliams, J. C., and Doney, S. C.: Oceanic vertical mixing: A review and a model with a nonlocal boundary layer parameterization, *Rev. Geophys.*, **32**, 363–403, 1994. 589, 591
- 30 Large, W. G., Danabasoglu, G., McWilliams, J. C., Gent, P. R., and Bryan, F. O.: Equatorial circulation of a global ocean climate model with anisotropic horizontal viscosity, *J. Phys. Oceanogr.*, **31**, 518–536, 2001. 589, 591

Failure analysis of climate simulation crashes

D. D. Lucas et al.

Title Page

Abstract

Introduction

Conclusions

References

Tables

Figures

⏪

⏩

◀

▶

Back

Close

Full Screen / Esc

Printer-friendly Version

Interactive Discussion



Lucas, D. D. and Prinn, R. G.: Parametric sensitivity and uncertainty analysis of dimethylsulfide oxidation in the clear-sky remote marine boundary layer, *Atmos. Chem. Phys.*, 5, 1505–1525, doi:10.5194/acp-5-1505-2005, 2005. 601

The HadGEM2 Development Team: Martin, G. M., Bellouin, N., Collins, W. J., Culverwell, I. D., Halloran, P. R., Hardiman, S. C., Hinton, T. J., Jones, C. D., McDonald, R. E., McLaren, A. J., O'Connor, F. M., Roberts, M. J., Rodriguez, J. M., Woodward, S., Best, M. J., Brooks, M. E., Brown, A. R., Butchart, N., Dearden, C., Derbyshire, S. H., Dharssi, I., Doutriaux-Boucher, M., Edwards, J. M., Falloon, P. D., Gedney, N., Gray, L. J., Hewitt, H. T., Hobson, M., Huddleston, M. R., Hughes, J., Ineson, S., Ingram, W. J., James, P. M., Johns, T. C., Johnson, C. E., Jones, A., Jones, C. P., Joshi, M. M., Keen, A. B., Liddicoat, S., Lock, A. P., Maidens, A. V., Manners, J. C., Milton, S. F., Rae, J. G. L., Ridley, J. K., Sellar, A., Senior, C. A., Totterdell, I. J., Verhoef, A., Vidale, P. L., and Wiltshire, A.: The HadGEM2 family of Met Office Unified Model climate configurations, *Geosci. Model Dev.*, 4, 723–757, doi:10.5194/gmd-4-723-2011, 2011. 586

Marzban, C.: The ROC curve and the area under it as performance measures, *Weather Forecast.*, 124, 1106–1113, 2004. 597

National Research Council Report: Assessing the Reliability of Complex Models: Mathematical and Statistical Foundations of Verification, Validation, and Uncertainty Quantification, The National Academies Press, 2012. 587

Pipitone, J. and Easterbrook, S.: Assessing climate model software quality: a defect density analysis of three models, *Geosci. Model Dev.*, 5, 1009–1022, doi:10.5194/gmd-5-1009-2012, 2012. 587

Platt, J. C.: Probabilistic outputs for support vector machines and comparisons to regularized likelihood methods, in: *Advances in Large Margin Classifiers*, MIT Press, 61–74, 1999. 594

Prati, R. C., Batista, G. E. A. P. A., and Monard, M. C.: Class imbalances versus class overlapping: an analysis of a learning system behavior, in: *MICAI*, edited by: Monroy, R., Arroyo-Figueroa, G., Sucar, L. E., and Azuela, J. H. S., *Lecture Notes in Computer Science*, vol. 2972, Springer, 312–321, 2004. 592

Randall, D., Wood, R., Bony, S., Colman, R., Fichet, T., Fyfe, J., Kattsov, V., Pitman, A., Shukla, J., Srinivasan, J., Stouffer, R., Sumi, A., and Taylor, K.: Climate Models and Their Evaluation, in: *Climate Change 2007: The Physical Science Basis, Contribution of Working Group I to the Fourth Assessment Report of the Intergovernmental Panel on Climate*

Failure analysis of climate simulation crashes

D. D. Lucas et al.

Title Page

Abstract

Introduction

Conclusions

References

Tables

Figures

◀

▶

◀

▶

Back

Close

Full Screen / Esc

Printer-friendly Version

Interactive Discussion



- Change, edited by: Solomon, S., Qin, D., Manning, M., Chen, Z., Marquis, M., Averyt, K. B., Tignor, M., and Miller, H. L., Cambridge University Press, 2007. 586
- Rugaber, S., Dunlap, R., Mark, L., and Ansari, S.: Managing software complexity and variability in coupled climate models, *IEEE Software*, 28, 43–48, 2011. 586
- 5 Saltelli, A., Chan, K., and Scott, E. M.: *Sensitivity Analysis*, Wiley, 2000. 600
- Smith, R., Jones, P., Briegleb, B., Bryan, F., Danabasoglu, G., Dennis, J., Dukowicz, J., Eden, C., Fox-Kemper, B., Gent, P., Hecht, M., Jayne, S., Jochum, M., Large, W., Lindsay, K., Maltrud, M., Norton, N., Peacock, S., Vertenstein, M., and Yeager, S.: *The Parallel Ocean Program (POP) reference manual, ocean component of the Community Climate System Model (CCSM)*, Tech. Rep. LAUR-10-01853, Los Alamos National Laboratory, 141 pp., 2010. 589, 591
- 10 Smith, R. D. and McWilliams, J. C.: Anisotropic horizontal viscosity for ocean models, *Ocean Model.*, 5, 129–156, 2003. 589, 591
- Sobol, I. M.: Global sensitivity indices for nonlinear mathematical models and their Monte Carlo estimates, *Math. Comput. Simulat.*, 55, 271–280, 2001. 600
- 15 Stensrud, D. J.: *Parameterization Schemes: Keys to Understanding Numerical Weather Prediction Models*, Cambridge University Press, 2009. 588
- Sudret, B.: Global sensitivity analysis using polynomial chaos expansions, *Reliab. Eng. Syst. Safe.*, 93, 964–979, 2008. 601
- 20 Swets, J. A.: Measuring the accuracy of diagnostic systems, *Science*, 240, 1285–1293, 1988. 596
- Tannahill, J., Lucas, D. D., Domyancic, D., Brandon, S., and Klein, R.: Data intensive uncertainty quantification: Applications to climate modeling, in: *Poster Presented at Super Computing 11*, November 12–18, Seattle, Washington, USA, doi:10.1145/2148600.2148610, 2011. 590
- 25 Tatang, M., Pan, W., Prinn, R., and McRae, G.: An efficient method for parametric uncertainty analysis of numerical geophysical models, *J. Geophys. Res.*, 102, 21925–21932, 1997. 601
- Vapnik, V. N.: *The Nature of Statistical Learning Theory*, Springer, New York, NY, USA, 1995. 594
- Walter, K.: *Narrowing Uncertainties*, *Science & Technology Review*, available at: <https://str.llnl.gov/JulAug10/klein.html> (last access: 22 January 2013), archived on 22 January 2013: <http://www.webcitation.org/6DsDwCRxY>, 2010. 590
- 30 Washington, W. M. and Parkinson, C. L.: *An introduction to three-dimensional climate modeling*, University Science Books, 2nd Edn., 2005. 587

Wiener, N.: The homogeneous chaos, Am. J. Math., 60, 897–936, 1938. 601
Xiu, D. and Karnidakis, G. E. M.: The Wiener–Askey polynomial chaos for stochastic differential equations, SIAM J. Sci. Comput., 24, 619–644, 2002. 601

GMDD

6, 585–623, 2013

Failure analysis of climate simulation crashes

D. D. Lucas et al.

Title Page

Abstract

Introduction

Conclusions

References

Tables

Figures



Back

Close

Full Screen / Esc

Printer-friendly Version

Interactive Discussion



Failure analysis of climate simulation crashes

D. D. Lucas et al.

[Title Page](#)

[Abstract](#)

[Introduction](#)

[Conclusions](#)

[References](#)

[Tables](#)

[Figures](#)

⏪

⏩

◀

▶

[Back](#)

[Close](#)

[Full Screen / Esc](#)

[Printer-friendly Version](#)

[Interactive Discussion](#)



Table 1. Parameters Sampled in the CCSM4 Parallel Ocean Model.

Parameter ^a	[low, default, high]	Scale ^b	Module	Description
1 vconst_corr	[0.3, 0.6, 1.2] × 10 ⁷	lin	hmix_aniso	variable viscosity parameter (vconst.1, vconst.6)
2 vconst.2	[0.25, 0.5, 2.0]	log	hmix_aniso	variable viscosity parameter
3 vconst.3	[0.16, 0.16, 0.2]	lin	hmix_aniso	variable viscosity parameter
4 vconst.4	[0.5, 2.0, 10.0] × 10 ⁻⁸	log	hmix_aniso	variable viscosity parameter
5 vconst.5	[2, 3, 5]	lin	hmix_aniso	variable viscosity parameter
6 vconst.7	[30.0, 45.0, 60.0]	lin	hmix_aniso	variable viscosity parameter
7 ah_corr	[2.0, 3.0, 4.0] × 10 ⁷	lin	hmix_gm	diffusion coefficient for Redi mixing (ah) and background horizontal diffusivity within the surface boundary layer (ah_bkg.srfbl)
8 ah_bolus	[2.0, 3.0, 4.0] × 10 ⁷	lin	hmix_gm	diffusion coefficient for bolus mixing
9 slm_corr	[0.05, 0.3, 0.3]	log	hmix_gm	maximum slope for bolus (slm_b) and Redi terms (slm_r)
10 efficiency_factor	[0.05, 0.07, 0.1]	lin	mix_submeso	efficiency factor for submesoscale eddies
11 tidal_mix_max	[25.0, 100.0, 200.0]	log	tidal	tidal mixing threshold
12 vertical_decay_scale	[2.5, 5.0, 20.0] × 10 ⁴	log	tidal	vertical decay scale for tide induced turbulence
13 convect_corr	[1.0, 10.0, 50.0] × 10 ³	log	vertical_mix	tracer (convect_diff) and momentum (convect_visc) mixing coefficients in diffusion option
14 bckgrnd_vdc1	[0.032, 0.16, 0.8]	log	vmix_kpp	base background vertical diffusivity
15 bckgrnd_vdc_ban	[0.5, 1.0, 1.0]	lin	vmix_kpp	Banda Sea diffusivity
16 bckgrnd_vdc_eq	[0.01, 0.01, 0.5]	log	vmix_kpp	equatorial diffusivity
17 bckgrnd_vdc_psim	[0.1, 0.13, 0.5]	log	vmix_kpp	maximum PSI induced diffusivity
18 Prandtl	[4.0, 10.0, 20.0]	log	vmix_kpp	ratio of background vertical viscosity and diffusivity

^a Individual `_corr` parameters (numbers 1, 7, 9, and 13) are used to represent the correlated pair of parameters given in the description. For example, values drawn for `vconst_corr` are assigned to `vconst.1` and `vconst.6`.

^b Linear and logarithmic scales are used for parameter ranges that have ratios of high/low < 5 and high/low ≥ 5, respectively.

Failure analysis of climate simulation crashes

D. D. Lucas et al.

Title Page

Abstract

Introduction

Conclusions

References

Tables

Figures



Back

Close

Full Screen / Esc

Printer-friendly Version

Interactive Discussion



Table 2. Latin Hypercube Studies of the CCSM4 Parallel Ocean Program.

Study	Simulations	Successes	Failures	Failure rate
1	180	160	20	11.1 %
2	180	168	12	6.7 %
3	180	166	14	7.8 %
Total	540	494	46	8.5 %

Failure analysis of climate simulation crashes

D. D. Lucas et al.

Title Page	
Abstract	Introduction
Conclusions	References
Tables	Figures
◀	▶
◀	▶
Back	Close
Full Screen / Esc	
Printer-friendly Version	
Interactive Discussion	

Table 4. Polynomial chaos expansion of failure probability.

Expansion	Leading terms*
ξ_i	$\log \mu_c \approx -4.347 + 4.049 \xi_1 + 3.400 \xi_2 + 2.267 \xi_{13} - 1.980 \xi_{14} - 1.393 \xi_{16} - 1.253 \xi_5 - 1.143 \xi_4 - 1.007 \xi_{17} - 0.885 \xi_2 \xi_1 - 0.796 \xi_{13} \xi_1 - 0.739 \xi_6 - 0.637 \xi_{13} \xi_2 - 0.610 \xi_9 + 0.578 \xi_{14} \xi_2 + 0.480 \xi_{16} \xi_2 - 0.471 \xi_{15} - 0.414 \xi_1^2 + 0.382 \xi_5 \xi_1 + 0.372 \xi_{14} \xi_1 + 0.351 \xi_{17} \xi_2 + 0.320 \xi_2 \xi_5 + 0.320 \xi_8^2 + \dots$
$P_n(\xi_i)$	$\log \mu_c \approx -2.609 + 1.628P_1(\xi_1) + 1.546P_1(\xi_2) + 1.061P_1(\xi_{13}) - 0.895P_1(\xi_{14}) - 0.475P_1(\xi_5) - 0.455P_1(\xi_{16}) - 0.338P_1(\xi_4) - 0.311P_1(\xi_{17}) - 0.245P_1(\xi_9) - 0.221P_1(\xi_1)P_1(\xi_2) - 0.199P_1(\xi_1)P_1(\xi_{13}) + 0.196P_1(\xi_{12}) + 0.174P_1(\xi_{10}) + 0.164P_1(\xi_{11}) - 0.159P_1(\xi_2)P_1(\xi_{13}) + 0.145P_1(\xi_2)P_1(\xi_{14}) + 0.133P_1(\xi_{18}) + 0.120P_1(\xi_2)P_1(\xi_{16}) + 0.096P_1(\xi_1)P_1(\xi_5) + 0.093P_1(\xi_1)P_1(\xi_{14}) + 0.088P_1(\xi_2)P_1(\xi_{17}) - 0.082P_1(\xi_6) + \dots$

*Leading terms are based on the magnitude of the absolute value of the coefficients of the polynomial chaos expansion. Refer to Table 1 for the parameter labels that correspond to the numbers.



Failure analysis of climate simulation crashes

D. D. Lucas et al.

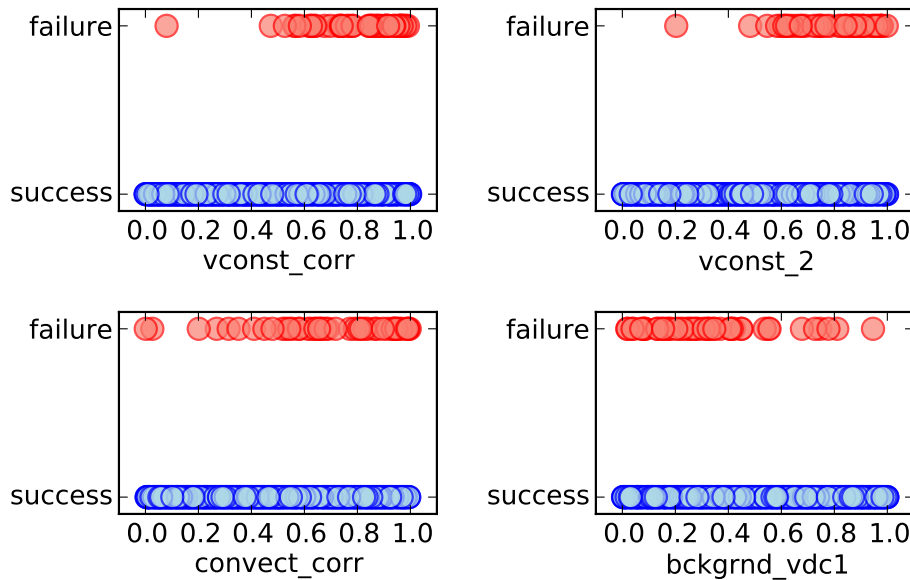


Fig. 1. Climate model simulation successes and failures are shown for one-dimensional projections of the values of 4 ocean parameters in 540 Latin hypercube experiments that sampled 18 model parameters. Parameter values are normalized using the ranges in Table 1.

Title Page

Abstract Introduction

Conclusions References

Tables Figures

⏪ ⏩

◀ ▶

Back Close

Full Screen / Esc

Printer-friendly Version

Interactive Discussion



**Failure analysis of
climate simulation
crashes**

D. D. Lucas et al.

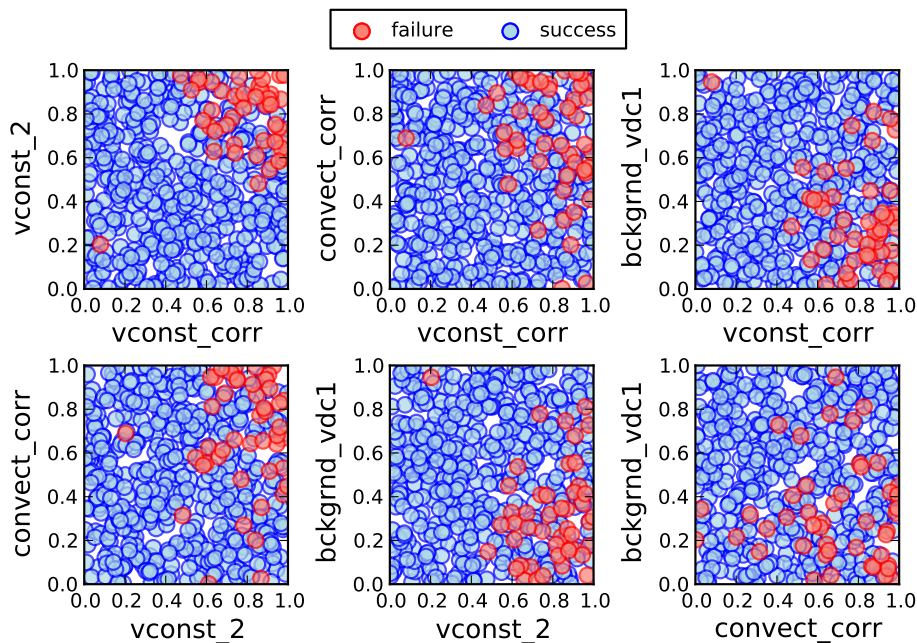


Fig. 2. Same as Fig. 1, but showing the two-dimensional projections for the same four model parameters.

[Title Page](#)[Abstract](#)[Introduction](#)[Conclusions](#)[References](#)[Tables](#)[Figures](#)[◀](#)[▶](#)[◀](#)[▶](#)[Back](#)[Close](#)[Full Screen / Esc](#)[Printer-friendly Version](#)[Interactive Discussion](#)

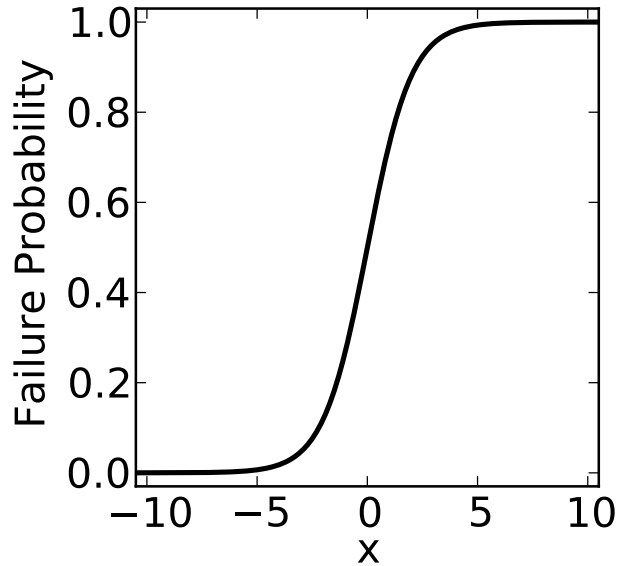


Fig. 3. Logistic sigmoid function defined in Eq. (3) with $\lambda(x) = x$.

**Failure analysis of
climate simulation
crashes**

D. D. Lucas et al.

Title Page

Abstract

Introduction

Conclusions

References

Tables

Figures



Back

Close

Full Screen / Esc

Printer-friendly Version

Interactive Discussion



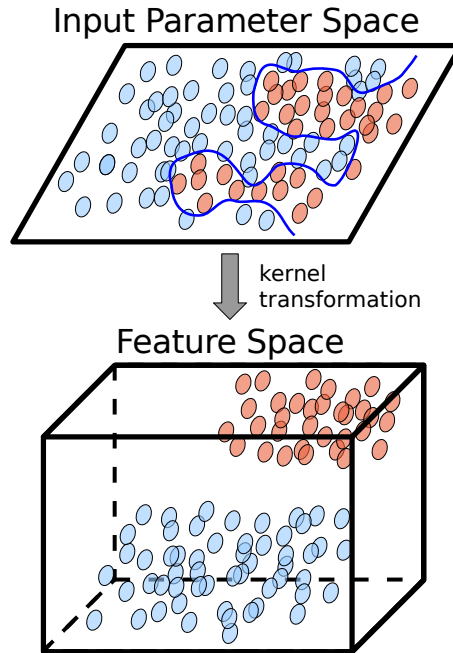


Fig. 4. Conceptual image showing the separability of the red and blue classes through kernel transformations in SVMs.

**Failure analysis of
climate simulation
crashes**

D. D. Lucas et al.

Title Page

Abstract

Introduction

Conclusions

References

Tables

Figures

◀

▶

◀

▶

Back

Close

Full Screen / Esc

Printer-friendly Version

Interactive Discussion



		Actual	
		Failure	Success
Predicted	Failure	True Positive (TP)	False Positive (FP)
	Success	False Negative (FN)	True Negative (TN)

$TPR = TP / (TP + FN)$		$FPR = FP / (FP + TN)$
------------------------	--	------------------------

Fig. 5. The confusion matrix showing the four possible outcomes for a two-class simulation failure problem.

Failure analysis of climate simulation crashes

D. D. Lucas et al.

[Title Page](#)

[Abstract](#) [Introduction](#)

[Conclusions](#) [References](#)

[Tables](#) [Figures](#)

[◀](#) [▶](#)

[◀](#) [▶](#)

[Back](#) [Close](#)

[Full Screen / Esc](#)

[Printer-friendly Version](#)

[Interactive Discussion](#)



**Failure analysis of
climate simulation
crashes**

D. D. Lucas et al.

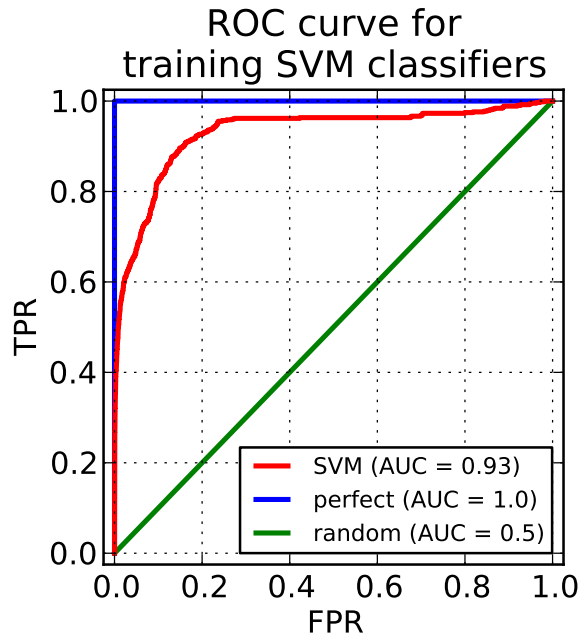


Fig. 6. Receiver operating characteristic for the bootstrapped set of individual SVM classifiers assessed using holdout test data. SVM training parameters ($\gamma = 0.1$, $C = 3$) are chosen to maximize the area under the ROC curve.

[Title Page](#)[Abstract](#)[Introduction](#)[Conclusions](#)[References](#)[Tables](#)[Figures](#)[◀](#)[▶](#)[◀](#)[▶](#)[Back](#)[Close](#)[Full Screen / Esc](#)[Printer-friendly Version](#)[Interactive Discussion](#)

		Actual	
		Failure	Success
Predicted	Failure	TP $D_{avg} = 9$ $D_{sum} = 11$ $D_{snr} = 12$	FP $D_{avg} = 1$ $D_{sum} = 3$ $D_{snr} = 2$
	Success	FN $D_{avg} = 5$ $D_{sum} = 3$ $D_{snr} = 2$	TN $D_{avg} = 165$ $D_{sum} = 163$ $D_{snr} = 164$
		14 actual failures	166 actual successes

Fig. 7. The confusion matrix for 180 independent validation simulations using the SVM committee with three different decision criteria (D_{avg} , D_{sum} , and D_{snr}).

Failure analysis of climate simulation crashes

D. D. Lucas et al.

[Title Page](#)

[Abstract](#) [Introduction](#)

[Conclusions](#) [References](#)

[Tables](#) [Figures](#)

[⏪](#) [⏩](#)

[◀](#) [▶](#)

[Back](#) [Close](#)

[Full Screen / Esc](#)

[Printer-friendly Version](#)

[Interactive Discussion](#)



Failure analysis of climate simulation crashes

D. D. Lucas et al.

Title Page

Abstract

Introduction

Conclusions

References

Tables

Figures



Back

Close

Full Screen / Esc

Printer-friendly Version

Interactive Discussion

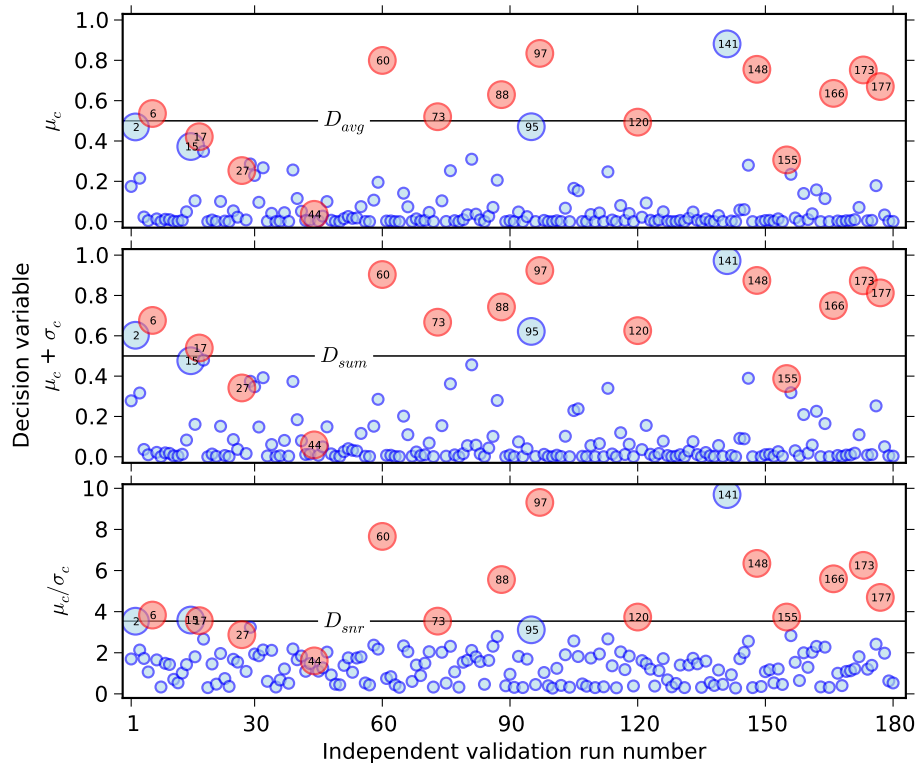


Fig. 8. Actual and predicted climate model simulation outcomes are shown for the 180 independent validation experiments. Predictions are based on three decision variables and thresholds (μ_c and D_{avg} , top; $\mu_c + \sigma_c$ and D_{sum} , middle; μ_c/σ_c and D_{snr} , bottom). The horizontal axis displays simulation numbers based on their order in the ensemble. Actual failures and successes are shown in red and blue, respectively. Larger symbols with the labeled run numbers highlight true positives and misclassifications (false positives and false negatives) by one or more of the criteria.

Failure analysis of climate simulation crashes

D. D. Lucas et al.

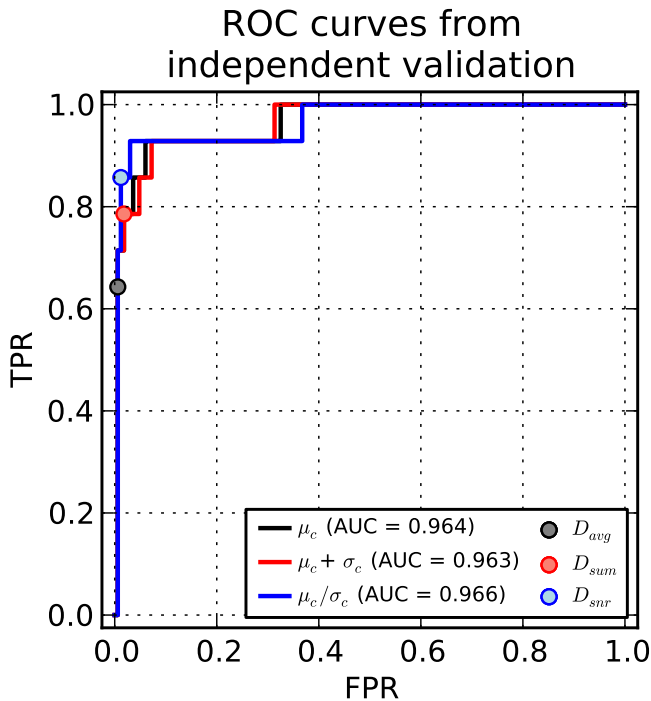


Fig. 9. ROC curves for the 180 independent validation climate model simulations using the SVM committee with three decision variables (μ_c , $\mu_c + \sigma_c$, and μ_c / σ_c). The locations of the discriminators using the fixed thresholds in D_{avg} , D_{sum} , and D_{snr} are also shown.

Discussion Paper | Discussion Paper | Discussion Paper | Discussion Paper | Discussion Paper

Title Page

Abstract

Introduction

Conclusions

References

Tables

Figures



Back

Close

Full Screen / Esc

Printer-friendly Version

Interactive Discussion



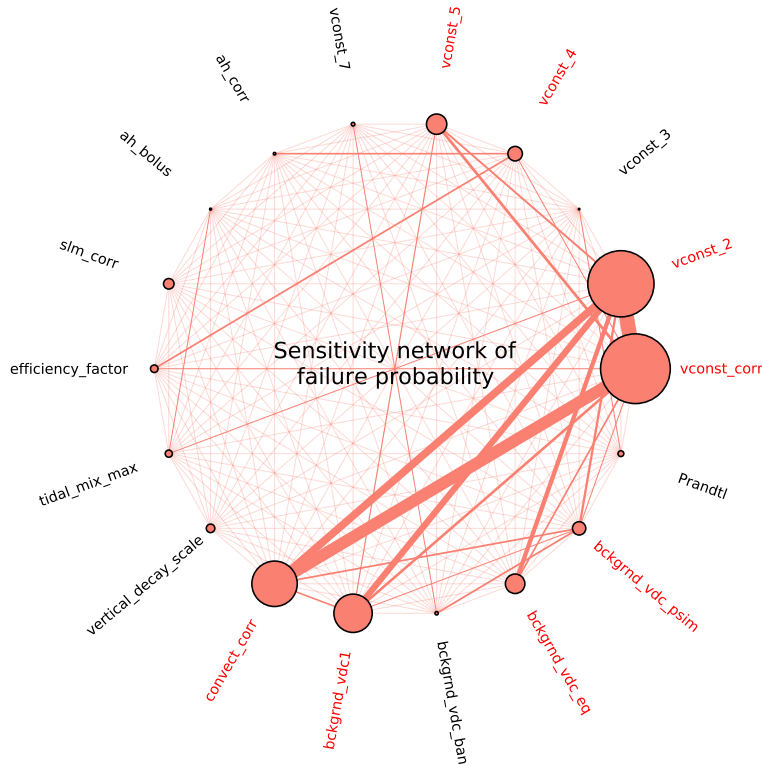


Fig. 10. Sensitivity of the probability of simulation failure to climate model parameters is shown using a network graph. Node size and connector thickness are proportional to sensitivity contributions from individual parameters and pairs of parameters, respectively. The eight parameters labeled in red are the main causes of simulation failures.

Failure analysis of climate simulation crashes

D. D. Lucas et al.

Title Page

Abstract Introduction

Conclusions References

Tables Figures

◀ ▶

◀ ▶

Back Close

Full Screen / Esc

Printer-friendly Version

Interactive Discussion

